A kinetic model for the anodic dissolution of Ti in HF in the active and passive regions

Authors: Fathima Fasmin, B.V.S. Praveen, S. Ramanathan*

Address: Department of Chemical Engineering, Indian Institute of Technology-Madras, Chennai 600036, India

Phone: +91 44 22574171

Fax: +91 44 2257 0509 (Attn: S. Ramanathan)

Email: srinivar@iitm.ac.in

* corresponding author

Abstract

We investigated the anodic dissolution of polycrystalline titanium rotating disc electrode in 0.1 M hydrofluoric acid in active and passive regions using potentiodynamic polarization and electrochemical impedance spectroscopy. In the active region, complex plane plots of the impedance spectra exhibited three capacitive loops indicting the presence of at least two adsorbed intermediates. In the passive region, they exhibited a negative resistance and a low frequency inductive loop. The high frequency loops exhibit constant phase element behavior indicating that a heterogeneous 2D film with partial surface coverage is present in the active and passive regions. The impedance data was fit to a reaction model and a four step mechanism with two adsorbed intermediate species is proposed to explain the observed trends in the active and passive regions. The change in the surface coverage of the adsorbed intermediate species, with the overpotential is estimated. This model describes the dissolution of Ti via two parallel paths, viz. a chemical step and an electrochemical step. The onset of passivation ensues when the rate of TiO_2 film formation is more than that of its dissolution. Transpassive dissolution becomes dominant when the electrochemical dissolution from the bare surface becomes negligible.

Key words: Titanium; Hydrofluoric acid; electrochemical impedance spectroscopy; passivation

1. Introduction:

Titanium metal and its alloys are widely used in engineering applications and medical implants, due to their low density, high corrosion resistance and high strength[1]. These materials possess excellent corrosion resistance in acidic media, through the formation of protective oxide film on the metal surface. In order to facilitate the attack of the passive oxide layer, solutions containing fluoride ions are used for the anodic dissolution of titanium[2-4]. The corrosion studies of titanium show that at low overpotentials, the dissolution is in active region, and at moderate overpotentials, surface passivation occurs. At high overpotentials, transpassive dissolution is observed.

The dissolution mechanism of titanium in solutions, with and without fluoride ions have been characterized using various techniques. The dissolution of Ti in 10M H_2SO_4 was investigated using polarization and impedance techniques[5] and it was reported that the dissolved species is Ti^{3+}. To the best of our knowledge, the earliest report on electrochemical studies of Ti dissolving in acidic fluoride ions was published by Kelly[6]. Polarization studies show clear active, passive and transpassive regions[6]. The impedance spectrum was acquired in the transpassive region and was analyzed to show that the film thickness increased with the potential[6]. The impedance of Ti in solutions containing strong acids (H_2SO_4 and HNO_3) along with 0.1 mM -10 mM hydrofluoric acid was analyzed[4] and a four step reaction mechanism involving Ti^{+}, Ti^{2+} and Ti^{3+} adsorbed intermediate species and Ti^{3+} dissolved species was proposed to explain the results. In each case, the spectra were acquired at only one potential. The confidence in the model identification would be enhanced if impedance data acquired at various *dc* potentials are employed in the analysis Besides, although it is possible for Ti to exist in +1 oxidation state[7], it is not very

common. Frateur et al. analyzed the formation of oxide layers on Ti in acidic fluoride solutions using electrochemical impedance spectroscopy[8]. They showed that the oxide layer thickness at various potentials can be estimated from the high frequency capacitance while the variation of oxide thickness with potential can be obtained from the low frequency capacitance values. The anodic oxidation of Ti in F^- containing acidic solutions was studied using impedance spectroscopy[9]. At open circuit potential (OCP), two capacitive loops were obtained, at various concentrations of fluoride ions. The reaction was modeled using a mechanism with four steps. In the impedance spectra of valve metals in fluoride solutions in transpassive region, low frequency capacitance is often observed and this was explained as due to the accumulation of the fluoride ions in the metal –film interface[10]. The impedance study of Ti dissolving in acidic fluoride solution at large positive potentials, i.e. in transpassive region, was reported[11] and the nature of the oxide film formed on the surface was elucidated. Another report[12] presented the impedance spectrum of Ti in fluoride solution in transpassive region (5 V *vs.* saturated calomel electrode), and proposed a reaction mechanism with two steps to model the dissolution. Recently, the anodic dissolution of Ti and its alloys in glycol with controlled H_2O and fluoride concentration was studied[13]. When the presence of dissolved oxygen and water is limited, passive region is not seen in polarization curves. The oxide formation and dissolution is modeled using a kinetic model with vacancy conduction in the film. Thus there are many reports which present the results of transpassive dissolution of Ti in fluoride solution, but the mechanism of Ti dissolution in the active and passive region is not well understood.

Electrochemical impedance spectroscopy (EIS) is one of the principal techniques capable of *in-situ* analysis of interfacial reaction and passivation mechanism[14-17]. It allows determining the

faradaic processes and other phenomena such as ion adsorption or diffusion which cannot be easily detected by other electrochemical techniques. The small amplitude signals used in EIS enables the measurement of the electrode properties without disturbing the system. By combining the two EIS analysis methods *viz.* electrical equivalent circuit (EEC) fitting analysis and reaction mechanism analysis, one can extract all the physical information contained in the impedance diagrams[18]. The goal of this work is to obtain the mechanism of dissolution of Ti in HF solution, in particular in the active and passive regions. Potentiodynamic polarization study of Ti dissolving in HF was performed. The impedance spectra were acquired at various *dc* potentials, viz. in the active, passive and transpassive regions. The EIS data were then subjected to both EEC and reaction mechanism analysis.

2. Experimental Section

A standard three electrode cell connected to PARSTAT 2263 (Princeton Applied Research) electrochemical workstation was used to conduct the electrochemical experiments. All experiments were carried out using a rotating disc electrode (RDE) embedded in a Teflon holder. The working electrode was made of a titanium rod (Ti 99.9%, Sigma-Aldrich) of 5 mm diameter. The disc rotation speed was maintained at 900 rpm using Pine Instruments RDE setup. A platinum wire was used as the counter electrode and Ag/AgCl (saturated KCl) was used as the reference electrode. The electrolyte contained 100mM HF acid, and 1 M Na_2SO_4 was used as the supporting electrolyte. Prior to each run, the electrode was mechanically polished with successively finer grades of grit paper, rinsed with ethanol and ultrasonicated to remove adhered particles. The experiments were conducted at room temperature, at natural pH of the solution (~2.3). The polarization curve was obtained by scanning the potential from OCP to 1500 mV

above OCP, at a scan rate of 10 mV/s. The impedance data were obtained by applying an ac perturbation of 10 mV (*rms*) superimposed on various *dc* potentials. The frequency range employed was from 30 kHz to 100 mHz, with 7 frequencies per decade (logarithmically spaced).

3. Results and Discussion

3.1 Potentiodynamic Polarization

Figure 1 shows the potentiodynamic polarization curve of Ti in a solution containing 100mM HF and 1M Na_2SO_4. The OCP was -1 V *vs.* Ag/AgCl. Experiments performed at a lower sweep rate of 2 mV/s yielded the same data, suggesting that the contribution from double layer charging current to the total current is very small and that the potentiodynamic polarization curve approximates the steady state behavior. Initially there is a substantial increase in current with the potential. Near a potential +400 mV *vs.* OCP, the current reaches a maximum, and further increase in potential causes the current to decrease. Similar anodic current peaks are observed for other valve metals such as Nb[19,20] or Ta[21] in fluoride media. Here, the region from 0 mV to 400 mV *vs.* OCP can be considered as active and from 400 mV to 850 mV *vs.* OCP can be considered as passive. In the active dissolution region, we can deduce that there is no passivating film on the electrode surface. In the passivating region, a film, either in 2 or 3 dimensions, would be present on the surface, but it may or may not completely cover the surface. At potential greater than 850 mV *vs.* OCP, the current shows a slight increase with potential, in the transpassive dissolution region. Here, a passivating film, most likely of three dimensions, would be present on the surface, and the dissolution occurs by transport of ions and vacancies through the film.

3.2 Impedance:

3.2.1. Observations: Impedance was acquired in the active, passive and transpassive regions by applying an ac potential superimposed on a *dc* potential onto the cell (quasi potentiostatic mode). The impedance data in the active region are presented in the three dimensional plots, i.e. complex plane plots as well as plots of the real and imaginary components *vs.* frequency in Fig 2a and Fig 2b. The experimental data are shown as open circles in the figure. The complex plane plots are also shown in Fig. 2c. Three capacitive loops are seen in the active region, although they are not well separated in the mid and low frequency ranges. The high frequency loop would correspond to the double layer, while the loop in the mid and low frequency range would correspond to the faradaic processes. In all the spectra, the low frequency data have more noise, presumably due to the longer integration time required. The high frequency loop appears as a depressed semi-circle rather than a regular semi-circle and hence a constant phase element (CPE) is used to model the double layer. The data were validated using linear KKT method[22], which essentially fits Voigt elements with well-defined time constants to the data and evaluates the residues. For all the impedance data reported in this work, the residues were found to be less than 3%.

Fig. 3a and Fig. 3b show the three dimensional plots of impedance spectra obtained in the passive region. The corresponding complex plane plots are shown in Fig. 3c. The *dc* current decreases with *dc* potential (Fig 1) in this region. The high frequency part of impedance spectra exhibits a capacitive behavior and the mid frequency region exhibits a capacitive behavior with a negative resistance. The low frequency impedance values exhibit an inductive behavior. Zsimpwin® software (Princeton Applied Research, AMETEK, USA) was used to fit the EEC

parameters. The EEC modeling fits the low frequency data in the passive region only if an inductance (or negative resistance and capacitance) are employed. Impedance of other valve metals such as Ta or Nb in fluoride solutions[19,21] and electro oxidation of glucose[23] or methanol[24,25] are known to exhibit negative resistances. However, there is an important difference between the current results and the other results with Ta or Nb. In the mid frequency region, Ti electrode does not exhibit any inductive behavior while Ta in HF[21] or Nb in HF[19] showed a clear inductive behavior in that region. In case of Ti dissolving in HF, the inductive behavior appears only in the low frequency region. Fig. 4a and Fig. 4b show the three dimensional plots of impedance data in the transpassive dissolution region. The data are very similar to those reported in the literature for Ti , Ta or Nb dissolution in fluoride media in the transpassive region[8,10,19,20]. The high frequency and low frequency data exhibit a capacitive behavior while the mid frequency data exhibit inductive behavior. Very detailed analysis of the transpassive oxide impedance is available in the literature[8,10,19,20] and only the observations relevant for comparison with the impedance in the active and passive regions are discussed here.

3.2.2 EEC Modeling: The EIS spectra obtained in the active and passive regions were fitted with the circuit given in Fig. 5a while the data in the transpassive region was fitted with circuit given in Fig 5b. In the active region, all the resistive and capacitive elements were allowed only positive values. In the passive region, one of the Maxwell elements (i.e. R_3 and C_3), was allowed to admit negative values so that the low frequency inductance can be modeled. The resistance R_p was also allowed to admit negative values so that the negative differential impedance can be modeled.

The best fit results are presented in Table I. The solution resistance varied between 1.8 and 2 Ω−cm^2. The double layer is modeled using a CPE and the CPE exponent values vary between 0.77 and 0.89. All the values are significantly less than one, showing that the surface may be quite heterogeneous. CPE behavior can arise from surface disorder and roughness[26], structural and/or chemical non-uniformity[27], electrode porosity[28], surface reconstruction or deconstruction[29], sluggishness of the adsorption step[29] or if a film is present on the surface, then, from the variation of the film properties perpendicular to the surface[30,31]. In this particular case, surface heterogeneity is the likely cause of CPE behavior. The CPE exponent value is particularly low in the passive region, although such low values have been observed experimentally[26]. The polarization resistance is defined as $R_p = \lim_{\omega \to 0} Z_F$ where ω is the angular frequency and Z_F is the faradaic impedance. In the circuit given in Fig. 5a, it corresponds to the resistance R_p. In the active region, R_p increases slightly with the overpotential, and in the passive region, it is negative and it increases significantly with the overpotential. The polarization resistance can be visualized as the inverse of the slope of the current-potential plot, and as the potential moves from the active to passive region, the slope would change from positive value to zero to negative values. Depending on whether one approaches the peak from the left or the right side, the inverse of the slope would be either $+\infty$ or $-\infty$ respectively. A comparison of Figure 1 and the values in Table I shows that the R_p values are along the expected lines.

In the active dissolution region, as well as the passive region, the values of R_2 decrease with potential, while that of C_2 increases. The Maxwell elements are coupled and are related to the relaxation of the adsorbed intermediates. When one of them increases in value, the other element tends to decrease in its value. The values of R_3 decrease with potential in the active region, with a

corresponding increase in C_3 values. In the passive region, negative values are admitted to the R_3 and C_3 values and the (pseudo) inductive loop in the low frequencies is modeled successfully. The charge transfer resistance is defined as $R_{ct} = \lim_{\omega \to \infty} Z_F$. If the impedance data appears as well separated loops in the complex plane representation of the spectra, R_{ct} can be estimated from the location of intersection of the high frequency capacitive loop with the real axis. In the circuit given in Fig 5a, it can be calculated by evaluating the equivalent resistance with R_p, R_2 and R_3 being in parallel. The calculated R_{ct} are also shown in Table I. The charge transfer resistance decreases with overpotential in the active region, but increases with overpotential in the passive region.

The circuit in Fig 5b is fit to the data in transpassive region and the results are tabulated in Table II. Although a CPE was used to model the high frequency loop, the fitted CPE exponent values were exactly 1, indicating that the behavior is that of an ideal capacitor. The capacitance values is also quite low especially at higher potential (1.36μF cm^{-2}), and this is likely due to the oxide film and not due to the double layer capacitance. In this region, a 3D oxide layer is expected to be formed and the oxide capacitance will dominate the overall capacitance measured[19]. The fact that the CPE exponent is practically 1 in the transpassive region, but significantly less than 1 in the active and passive regions indicates that surface heterogeneity plays an important role in defining the impedance response at high frequencies, in the active and passive region. On the other hand, in the transpassive region the film quality and thickness appears to be more or less uniform both across the surface and perpendicular to the surface, as otherwise a CPE behavior would be exhibited by the film too[30,31]. The inductance exhibited by the impedance data in the mid frequency range can be assigned to the high frequency migration of major current carriers[13].

The charge transfer resistance increases with the potential, while the inductance (L_4) and the associated resistance(R_4) decrease with the potential. The capacitance (C_5) appearing at the low frequency is assigned either to the variation in film thickness with low frequency perturbations[19] or to the accumulation of fluoride ions in the metal- film interface[10]. While a pure capacitance would exhibit a vertical line in the complex plane plot, a capacitance (C_5) in parallel with a resistance (R_5) is required to model the data, since the complex plane plots show that the data at the low frequencies do show a variation of the real component of the impedance. The transpassive dissolution has been studied in detail[10,19,20] and other than the observation that the CPE values suggest that the surface is completely covered with a uniform oxide in the transpassive region, the focus of this work is limited to dissolution in the active and passive regions. While EEC is quite successful in modeling the data, assigning a physical meaning to the parameter values, especially the ones with negative sign, and extracting physically relevant information such as surface coverage of passivating film as a function of potential, and dissolution rates is a formidable task. A reaction mechanism analysis is employed to obtain better insight into the physical processes which occur during the dissolution of Ti in HF.

3.2.2. Reaction Mechanism Analysis:

The impedance spectra of Ti dissolving in fluoride media, acquired at OCP, has been modeled before. Kuchukbayev proposed the following reactions[4]

$$
\begin{aligned}
&Ti + HF \rightleftharpoons (TiF)_{ads} + H^+ + e^- \\
&(TiF)_{ads} + H_2O \rightleftharpoons (TiFHOH)^+_{ads} + e^- \\
&(TiFHOH)^+_{ads} \rightleftharpoons (TiOH)^{2+}_{ads} + HF + e^- \\
&2(TiOH)^{2+}_{ads} + HF + H^+ \rightarrow TiF^{2+} + Ti^{3+} + 2H_2O
\end{aligned}
\qquad (1)
$$

This involves Ti at oxidation state of +1, which is possible but is not quite common. Kong et al proposed another mechanism (Eqn. 2) to model EIS data at OCP[9]

$$\begin{aligned} &Ti \xrightarrow{k_1} (TiO^+_{ads}) + 3e^- \\ &(TiO^+_{ads}) \xrightarrow{k_2} (TiO^+_{aq}) \\ &Ti + xF^- \xrightarrow{k_3} TiF^{3-x}_{x-ads} + 3e^- \\ &TiF^{3-x}_{x-ads} \xrightarrow{k_4} TiF^{3-x}_{x-aq} \end{aligned} \qquad (2)$$

where k_2 and k_4 are independent of potential. Later, the dissolution in transpassive region (5 V *vs.* SCE) is modeled using kinetic mechanism proposed below[12]

$$Ti + (2 - 0.5x) H_2O + xF^- \xrightarrow{k_1} TiO_{2-0.5x}F_x + (4 - x) H^+ + 4e^- \qquad (3)$$

$$Ti + TiO_{2-0.5x}F_x + 6F^- \xrightarrow{k_2} TiF^{2-}_{6-aq} + TiO_{2-0.5x}F_x + 4e^-$$

In the last step, the intermediate species $TiO_{2-0.5x}F_x$ is regenerated and this is sometimes referred to as catalytic mechanism[32]. The mechanisms proposed in the existing literature suffer from the following shortcomings. They are based on data acquired at a single *dc* potential, either at OCP or in the transpassive region. It is important that the data must be obtained at different *dc* potentials, and modeled so that the confidence in the model can be enhanced[33]. At and near OCP, the reverse reactions must also be included except for the step producing soluble species, which would be removed if the solution is stirred or if a RDE is employed. In addition, the *dc* current values predicted by the simulation must be compared with the measured potentiodynamic polarization curves. In particular, the maximum in the current potential curve, marking the active to passive transition must be captured by the simulations.

To model the observed EIS data in the active and passive region, we propose the following reaction mechanism. The derivation of the mass and charge balance equations are given in the literature[16,32,34-36] and only the key steps are presented here.

$$
\begin{aligned}
&Ti \underset{k_{-1}}{\overset{k_1}{\rightleftharpoons}} Ti_{ads}^{3+} + 3e^- \\
&Ti_{ads}^{3+} \underset{k_{-2}}{\overset{k_2}{\rightleftharpoons}} Ti_{ads}^{4+} + e^- \\
&Ti_{ads}^{4+} \xrightarrow{k_3} Ti_{sol}^{4+} \\
&Ti_{ads}^{3+} \xrightarrow{k_4} Ti_{sol}^{4+} + e^-
\end{aligned}
\qquad (4)
$$

Note that the third step is a chemical reaction and hence the corresponding rate constant k_3 does not depend on the potential. The third and the fourth steps result in the actual dissolution of the metal, with the third being a chemical step while the fourth is an electrochemical step. Any mechanism proposed here must have at least two adsorbed intermediates since three time constants are present in the impedance data (Fig 2a). Double layer capacitance can account for one of the time constants, and two other time constants must be explained by the reaction. In developing the following equations, the assumptions are that mass transfer resistance is negligible, Langmuir isotherm model is applicable, kinetic rate constants of electrochemical steps are exponentially dependent on the potential and at 10 mV *rms* ac perturbation, the equations can be linearized. The species Ti_{ads}^{3+} and Ti_{ads}^{4+} may be present as an oxide (Ti_2O_3 or TiO_2) or fluoride (TiF_3 or TiF_4) or oxy-fluoride ($TiO_{1.5-0.5x}F_x$ or $TiO_{2-0.5x}F_x$) with partial surface coverage (i.e. film is 2D only). The soluble species will most likely be $\left[TiF_6\right]^{2-}$. The fractional surface coverage of Ti_{ads}^{3+} and Ti_{ads}^{4+} are denoted by θ_1 and θ_2 respectively. The total number of sites per unit area is given by Γ and the time is denoted by 't'.

The corresponding mass balance equations are

$$\Gamma \frac{d\theta_1}{dt} = k_1\left(1-\theta_1-\theta_2\right) - k_{-1}\theta_1 - k_2\theta_1 + k_{-2}\theta_2 - k_4\theta_1 \quad (5)$$

$$\Gamma \frac{d\theta_2}{dt} = k_2\theta_1 - k_{-2}\theta_2 - k_3\theta_2 \quad (6)$$

The steady state fractional surface coverage values can be calculated by setting the equations (5) and (6) to zero. The results are

$$\theta_{1-SS} = \frac{k_{1-dc}\left(k_{-2-dc}+k_3\right)}{\left(k_{1-dc}+k_{-1-dc}+k_{2-dc}+k_{4-dc}\right)\left(k_{-2-dc}+k_3\right)+k_{2-dc}\left(k_{1-dc}-k_{-2-dc}\right)} \text{ and} \quad (7)$$

$$\theta_{2-SS} = \frac{k_{2-dc}\theta_{1-SS}}{\left(k_{-2-dc}+k_3\right)} \quad (8)$$

Here, the subscript '*dc*' is used to indicate that the rate constant is evaluated at the potential V_{dc}, which is the potential *vs.* OCP at which the impedance was acquired, and the subscript '*SS*' denotes the steady state values. The faradaic current is given by

$$i_F = F\left[3\times\left(k_1\left(1-\theta_1-\theta_2\right)-k_{-1}\theta_1\right)+1\times\left(k_2\theta_1-k_{-2}\theta_2\right)+k_4\theta_1\right] \quad (9)$$

Under steady state conditions, we can write

$$i_{F-SS} = 4F\left[k_3\theta_{2-SS}+k_{4-dc}\theta_{1-SS}\right] \quad (10)$$

Equation (9) can be written in Taylor series and under small signal conditions, the higher order terms can be neglected. For example, $k_1 = k_{10}e^{b_1(V_{dc}+V_{ac})} \approx k_{10}e^{b_1V_{dc}}\left[1+b_1V_{ac}\right] = k_{1-dc}\left[1+b_1V_{ac}\right]$ and other rate constants can be written in a similar fashion. The surface coverage values can also be approximated as $\theta_i \approx \theta_{i-SS} + \frac{d\theta_i}{dV}V_{ac}$

Under small signal conditions, the faradaic impedance Z_F can be written as[9,12,23]

$$\left(Z_F\right)^{-1} = \frac{\Delta i_F\big|_\omega}{\Delta V\big|_\omega} = \left(R_{ct}\right)^{-1} - F\left\{\left[3\left(k_{1-dc}+k_{-1-dc}\right)-\left(k_{2-dc}+k_{4-dc}\right)\right]\frac{d\theta_1}{dV}+\left[3k_{1-dc}+k_{-2-dc}\right]\frac{d\theta_2}{dV}\right\} \quad (11)$$

where

$$\left(R_{ct}\right)^{-1} = F\begin{bmatrix} 3\left(b_1k_{1-dc}\left(1-\theta_{1-SS}-\theta_{2-SS}\right)-b_{-1}k_{-1-dc}\theta_{1-ss}\right)+ \\ 1\left(b_2k_{2-dc}\theta_{1-SS}-b_{-2}k_{-2-dc}\theta_{2-SS}+b_4k_{4-dc}\theta_{1-SS}\right)\end{bmatrix} \quad (12)$$

Expanding the equations (5) and (6) in Taylor series, truncating after the first order term and re-arranging, it can be shown that we would get

$$A1\frac{d\theta_1}{dV}+B1\frac{d\theta_2}{dV}=C1 \text{ and} \quad (13)$$

$$D1\frac{d\theta_1}{dV}+E1\frac{d\theta_2}{dV}=F1 \quad (14)$$

where

$$A1 = k_{1-dc}+k_{-1-dc}+k_{2-dc}+k_{4-dc}+j\omega\Gamma$$

$$B1 = \left(k_{1-dc}-k_{-2-dc}\right)$$

$$C1 = \left[b_1k_{1-dc}\left(1-\theta_{1-SS}-\theta_{2-SS}\right)-b_{-1}k_{-1-dc}\theta_{1-SS}-b_2k_{2-dc}\theta_{1-SS}+b_{-2}k_{-2-dc}\theta_{2-SS}-b_4k_{4-dc}\theta_{1-SS}\right]$$

$$D1 = -k_{2-dc}$$

$$E1 = k_{-2-dc}+k_3+j\omega\Gamma$$

$$F1 = \left(b_2k_{2-dc}\theta_{1-SS}-b_{-2}k_{-2-dc}\theta_{2-SS}\right)$$

Solving the linear equations (13) and (14) together, the derivatives of surface coverage with respect to the potential can be obtained and substituted in equation (11). An optimization code written in Matlab® was used to estimate the kinetic parameters. The *dc* current *vs. dc* potential was also simulated using the same model and compared with the experimental results. Only the impedance data in the active and passive regions are modeled since the transpassive region is

expected to have 3D oxide and have been analyzed extensively[10,19,20]. The best fit kinetic parameters are given in Table III.

The *dc* current *vs.* potential predicted from this model are shown as dashed lines in Fig. 1 and it is clear that they match reasonably well in the active and passive regions. In the transpassive region, the predicted dissolution rates are much lower than the actual rates (not shown) because the model does not take into account the transpassive dissolution through the oxide. The simulated impedance spectra are presented in Fig 6a-d in the active and passive regions. The values of R_{ct} and R_p predicted by the model are shown along with the EEC predictions in Table IV. The model impedance corresponding to the lowest frequency (100 mHz) is taken as the $R_{p\text{-}RMA}$. Although the simulated spectra do not exactly match the experimental data quantitatively in some of the frequencies, the following trends match well. The values of R_{ct} match well with the experimental results. The value of R_p increases with overpotential in both the active and passive regions. The main deficiency of the simulation is the inability to capture the low frequency inductive loop in the passive region. In the active region, the experimental data show three capacitive loops while the simulations show only two capacitive loops. A reaction with two adsorbed intermediates can yield three capacitive loops. However, if two of the three time constant values are close enough, then only one loop will manifest in the complex plane plot and that is the likely explanation for the observed pattern. In the passive region, RMA does not capture the low frequency inductive loop, and a similar issue has been observed earlier[32,34] . In the earlier work[32,34], the anodic dissolution of Cr rich alloy in 1M H_2SO_4 (pH =0) was studied using EIS. In the vicinity of maximum *dc* current, the complex plane plot of impedance was similar to that in Fig. 3c, i.e. the data exhibited a low frequency inductive loop, a capacitive loop

with a negative resistance in the mid frequency range and a high frequency capacitive loop. The model, involving an eight step reaction mechanism was able to capture the high frequency capacitive loop and the mid frequency capacitive loop with negative resistance, but the low frequency inductive loop was not captured. Although the EIS data match is not quantitative, most of the features of the spectra are captured adequately by the mechanism given in equation (4).

The surface coverage values of the adsorbed intermediate species as predicted by the model are shown in Fig. 7. The surface coverage of Ti_{ads}^{4+} species, which is most likely TiO_2, begins to increase mainly from an overpotential of 0.3 V and it reaches values close to 1 when the overpotential is 0.8 V. When the overpotential is close to 0.8 V, it is likely that 3D film formation occurs and the transpassive dissolution model has to be employed at higher potentials.

The dissolution rates, i.e. rate of formation of Ti_{sol}^{4+} by the chemical reaction via step 3 and electrochemical reaction via step 4 are plotted as a function of *dc* potential in Fig. 8. Near the active passive transition, the electrochemical dissolution rate is almost two orders of magnitude higher than the chemical dissolution rate. The major dissolution pathway, then, occurs via the oxidative dissolution of trivalent species of Ti. At an overpotential of 0.8 V, when Ti_{ads}^{4+} species surface coverage is almost complete, the surface is passivated. At higher potentials, the chemical dissolution is independent of the potential and transpassive dissolution, which increases with the potential, becomes dominant. Hydrofluoric acid is an aggressive fluid which limits the number of *in-situ* techniques that can be applied to probe the Ti dissolution in HF. In addition, Ti is very reactive and on exposure to air immediately forms a protective TiO_2 layer and hence the results

based on *ex-situ* methods are not easy to translate to the conditions during actual dissolution. The current study illustrates the effectiveness of EIS in unraveling the kinetics of challenging systems such as Ti dissolution in HF.

Conclusions: The dissolution of Ti in HF solution is characterized using potentiodynamic polarization and impedance spectra measurements. The spectra in the active, passive and transpassive region were modeled using equivalent electrical circuits. The spectra in the active and passive dissolution were also modeled using mechanistic analysis. A four step mechanism involving a trivalent and a tetravalent Ti intermediate species adequately models the polarization curve and the spectra in the active and passive regions. The Ti surface in the active and passive region exhibits significant heterogeneity. The dissolution occurs via a chemical step in parallel with an electrochemical step. The model predicts that up to an overpotential of 0.6 V, the surface does not have a complete passivating oxide and only a 2D film, partially covering the surface, is present. Above the overpotential of 0.8 V, the chemical dissolution remains constant, but the contribution from electrochemical dissolution becomes negligible. At higher overpotentials, complete passivation occurs and transpassive dissolution via the 3D film becomes important.

References:

1) R. Boyer, E. W. Collings and G.Welsch, *Materials Properties Handbook: Titanium Alloys*, 1st ed., ASM International: Materials Park, OH (1994)
2) M. E. Staumanis and P.C. Chen, *J. Electrochem. Soc*., **98**(6), 234 (1951)
3) W. Wilhelmsen and A. P. Grande, *Electrochim. Acta*, **32**(10), 1469 (1987)
4) K. G. Kuchukbayev and V. I. Kichigin, *Protection of Metals*, **30**(3), 246 (1994)
5) R. D. Armstrong and R. E. Firman*, J. Electroanal. Chem*., **34**, 391 (1972)
6) J. J.Kelly, *Electrochim. Acta,* **24,** 1273 (1979)
7) N. Andersson, W. J. Balfour, P. F. Bernath, B. Lindgren, and R. S.Ram, *J. Chem. Phys*., **118**, 3543（2003)
8) I. Frateur, S. Cattarin, M. Musiani and B. Tribollet*, J. Electroanal. Chem*., **482**, 202 (2000)
9) D. -S. Kong and Y.-Y. Feng, *J. Electochem. Soc*., **156** (9), C283 (2009)
10) D. -S. Kong, *Langmuir*, **26**(7), 4880 (2010)
11) P. Acevedo-Pena and I. Gonzalez, *J. Electochem. Soc*., **159**(3), C101 (2012)
12) D.-S. Kong, W.-Q. Kong, Y.-Y. Feng, W.-J. Li and Y.-J. Wei, *J. Electochem. Soc*., **160**(10), C461 (2013)
13) M. Bojinov and M. Stancheva, *J. Electroanal. Chem.,* **737**, 150 (2015)
14) E. Barsoukov and J. R. Macdonald, *Impedance Spectroscopy*, Second. Ed. John Wiley and Sons, New Jersey (1989)
15) M. Orazem and B. Tribollet, *Electrochemical Impedance Spectroscopy*, John Wiley and Sons, NJ, (2008)

16) D.D. Macdonald, S. Real, S.I. Smedley and M. Urquidi-Macdonald, *J. Electrochem. Soc*., **135**, 2410 (1988)

17) J. R. Macdonald*, J. Electroanal. Chem.*, **223**, 25 (1987)

18) D. D. Macdonald, *Electrochim. Acta,* **51**(8), 1376 (2006)

19) S. Cattarin, M. Musiani and B. Tribollet, *J. Electochem. Soc.***, 149**(10), B457 (2002)

20) M. Bojinov, S. Cattarin, M. Musiani, and B. Tribollet, *Electrochim. Acta*, **48**, 4107 (2003)

21) S. Sapra, H. Li, Z. Wang and I. I. Suni, *J. Electochem. Soc.*, **152(**6), B193 (2005)

22) B.A. Boukamp, *J. Electrochem. Soc.*, **142**, 1885 (1995)

23) I. Danaee, M. Jafarian, F. Forouzandeh, F. Gobal and M. G. Mahjani, *J. Phys. Chem. B*, **112** (49), 15933 (2008)

24) R. E. Melnick and G.T.R. Palmore, *J . Phys. Chem. B*, **105** (5), 1012 (2001)

25) R. E. Melnick and G.T.R. Palmore, *J. Phys. Chem. B,* **105** (39), 9449 (2001)

26) P. Córdoba-Torres, T.J. Mesquita, O. Devos, B. Tribollet, V. Roche and R.P. Nogueira, *Electrochim. Acta*, **72,** 172 (2012)

27) A.J. Motheo, A. Sadkowski and R.S. Neves, *J. Electroanal. Chem.*, **430,** 253 (1997)

28) C. Hitz and A. Lasia, *J. Electroanal. Chem.*, **500,** 213 (2001).

29) T. Pajkossy, *Solid State Ionics*, **94**, 123 (1997)

30) B. Hirschorn, M.E. Orazem, B. Tribollet, V. Vivier, I. Frateur and M. Musiani, *J. Electrochem Soc*., **157**, C452 (2010)

31) B. Hirschorn, M. E. Orazem, B. Tribollet , V.Vivier, I. Frateur and M.Musiani, *J. Electrochem. Soc.,* **157**, C458 (2010)

32) M. Keddam, O.R., Mattos and H. Takenouti, *Electrochim. Acta,* **31**, 1147 (1986)

33) S. Ramanathan, *ECS. Trans*., **33**, 21 (2011)

34) M. Keddam, O.R., Mattos and H. Takenouti, *Electrochim. Acta***, 31**,1159 (1986**)**

35) M. Bojinov, *J. Electroanal. Chem.*, **405,** 15 (1996)

36) J. Gregori, J. J. Garcia-Jareno, D. Gimenez-Romero, A. Roig and F. Vicente, *J. Electrochem. Soc.*, **154**, C371 (2007**)**

Table Captions

Table I: Best fit parameters for Ti dissolving in 100 mM HF in the active and passive regions. The circuit in Fig. 5a is used to model the data shown in Fig. 2 and Fig. 3

Table II: Best fit parameters for Ti in 100 mM HF in the transpassive region, using the circuit in Fig. 5b to model the data shown in Fig. 4

Table III. The best fit kinetic parameters used to model the data in Fig. 2 and Fig. 3 using the mechanism in equation (4)

Table IV: Comparison of the high frequency and low frequency limits of impedance based on RMA predictions with those based on EEC fit. The mechanism in equation (4) is employed for RMA while the circuit in Fig. 5a is employed for EEC.

Figure Captions

Figure 1 Potentiodynamic polarization graph of Ti in 100mM HF +1M Na_2SO_4. The continuous line represents the experimental data. The open circles represent the potential where impedance data were acquired. The dotted line represents the mechanistic simulation results.

Figure 2. Impedance data in the active region as three dimensional plots (a) OCP + 0.1 V (b) OCP + 0.2 V . (c) Complex plane plots of impedance at OCP + 0.1 V and OCP + 0.2 V. The points represent the experimental data and the lines represent the electrical equivalent circuit (EEC) model results.

Figure 3. Impedance data in the passive region as three dimensional plots (a) OCP + 0.45 V (b) OCP + 0.55 V. (c) Complex plane plots of impedance at OCP + 0.45 V and OCP + 0.55 V. The points represent the experimental data and the lines represent the electrical equivalent circuit (EEC) model results.

Figure 4. Impedance data in the transpassive region as three dimensional plots (a) OCP + 1 V, (b) OCP + 1.45 V. The points represent the experimental data and the lines represent the electrical equivalent circuit (EEC) model results.

Figure 5. Equivalent electrical circuits used to model the experimental impedance data in (a) active and passive regions and in (b) transpassive regions.

Figure 6. Mechanistic simulation results along with experimental data, in the active (a) OCP + 0.1 V (b) OCP + 0.2 V and passive (c) OCP + 0.45 V (d) OCP + 0.55 V regions. The points represent the experimental data and the lines represent the reaction mechanism analysis (RMA) results

Figure 7. Fractional surface coverage of Ti, Ti^{3+} and Ti^{4+} species as a function of potential (*vs.* OCP). The mechanistic pathway is given in equation (4) and the kinetic parameters are tabulated in Table III.

Figure 8. Dissolution of Ti in HF as a function of potential, via chemical (step 3 of equation 4) and electrochemical (step 4 of equation 4) paths

Tables

Table I

Potential (mV *vs.* OCP)	R_{sol} (Ω cm^2)	Y_0 (ohm^{-1}cm^{-2} S^n)	n	R_p (Ω cm^2)	C_2 (mF cm^{-2})	R_2 (Ω cm^2)	C_3 (mF cm^{-2})	R_3 (Ω cm^2)	$R_{ct\text{-}EEC}$ (Ω cm^2)
100	1.8	8.66×10^{-4}	0.84	8.1	8.2	23.1	1.9	5.9	3
200	1.9	4.28×10^{-4}	0.89	8.7	6.9	27.8	2.2	4.8	2.8
450	1.9	1.02×10^{-3}	0.78	-31.1	27.5	1.1	-30.6	-2.1	2.6
550	1.9	2.04×10^{-3}	0.77	-10.3	55.0	0.14	-55.5	-0.2	3.7

Table II

Potential (mV *vs.* OCP)	R_{sol} (Ω cm^2)	Y_0 (ohm^{-1}cm^{-2} S^n)	n	R_{ct} (Ω cm^2)	L_4 (mH cm^2)	R_4 (Ω cm^2)	C_5 (mF cm^{-2})	R_5 (Ω cm^2)
1000	2.0	2.17×10^{-5}	1	20.4	400	63.9	10.2	673
1450	1.9	1.36×10^{-6}	1	25.9	258	53.1	9.7	602

Table III

k_{10}	k_{20}	k_{30}	k_{40}	k_{-10}	k_{-20}	Γ	b_1	b_2	b_4	b_{-1}	b_{-2}
mol cm^{-2} s^{-1}						mol cm^{-2}	V^{-1}				
3.26×10^{-8}	2.11×10^{-7}	2.12×10^{-9}	8.95×10^{-8}	8.31×10^{-7}	5.11×10^{-4}	3.07×10^{-9}	7.3	0	0.5	-17.1	-14

Table IV

Potential (mV *vs.* OCP)	$R_{ct\text{-}EEC}$ (Ω cm^2)	$R_{ct\text{-}RMA}$ (Ω cm^2)	$R_{p\text{-}EEC}$ (Ω cm^2)	$R_{p\text{-}RMA}$ (Ω cm^2)
100	3	3	8.1	10.7
200	2.8	2.7	8.7	11
450	2.6	2.6	-31.1	-25.4
550	3.7	3.7	-10.3	-6

Figures

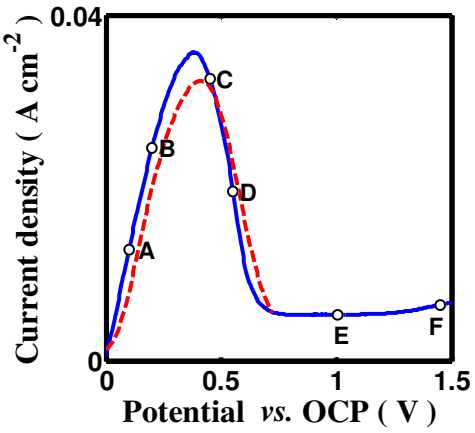

Fig. 1

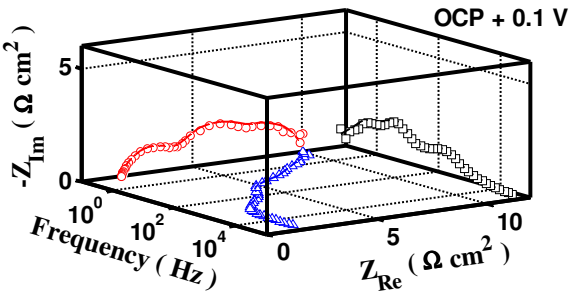

Fig. 2(a)

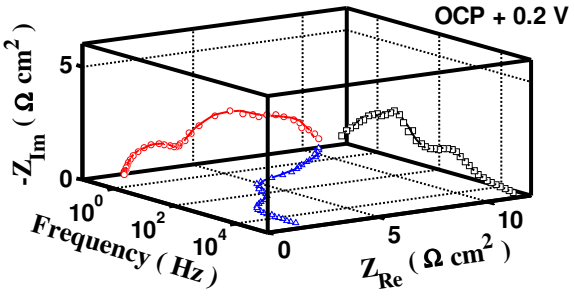

Fig. 2(b)

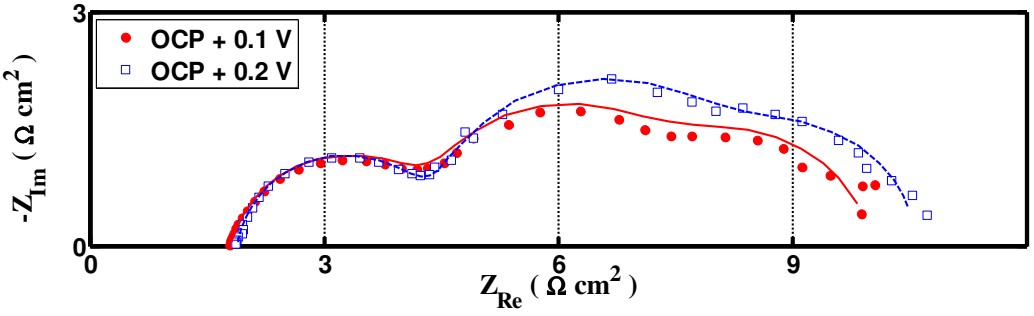

Fig. 2(c)

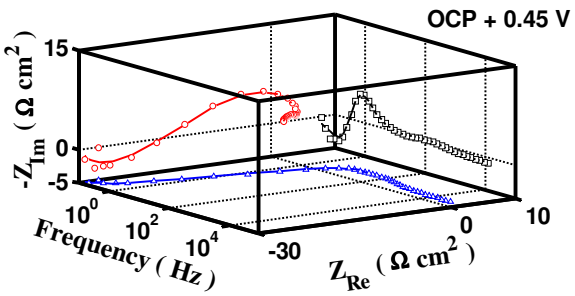

Fig. 3(a)

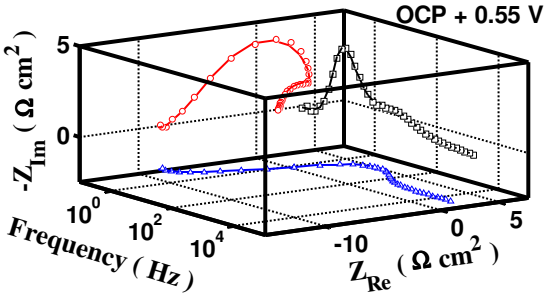

Fig. 3(b)

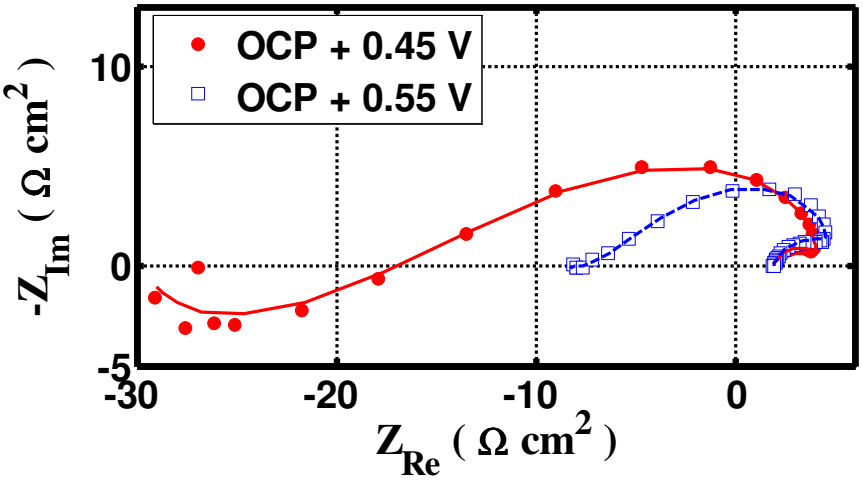

Fig. 3(c)

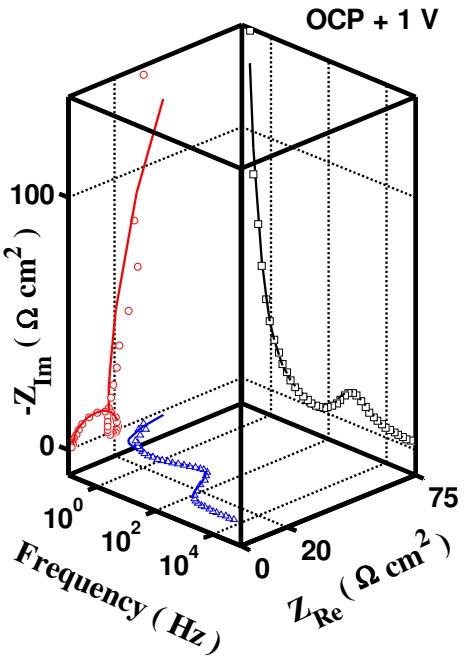
OCP + 1 V
100
0
-Z_Im (Ω cm^2)
10^0
10^2
10^4
Frequency (Hz)
0
20
75
Z_Re (Ω cm^2)

Fig. 4(a)

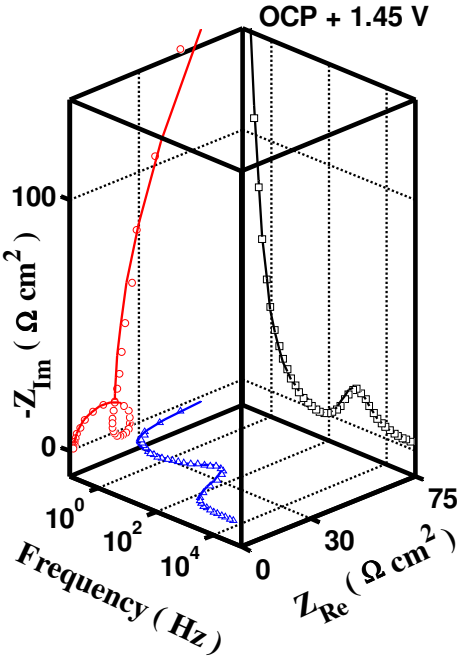
OCP + 1.45 V
100
0
-Z_Im (Ω cm^2)
10^0
10^2
10^4
Frequency (Hz)
0
30
75
Z_Re (Ω cm^2)

Fig. 4(b)

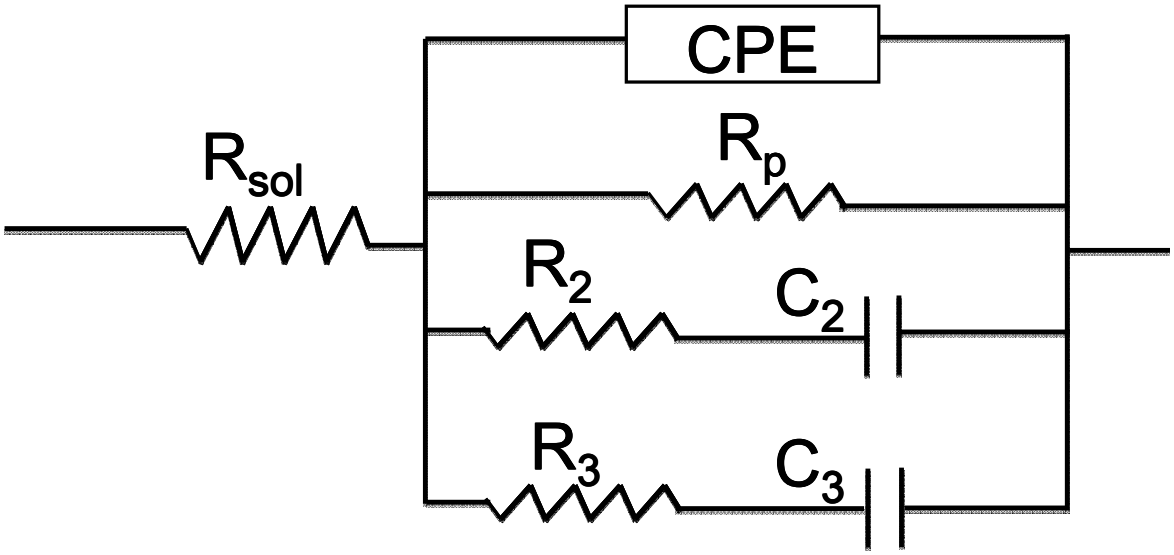

Fig. 5a

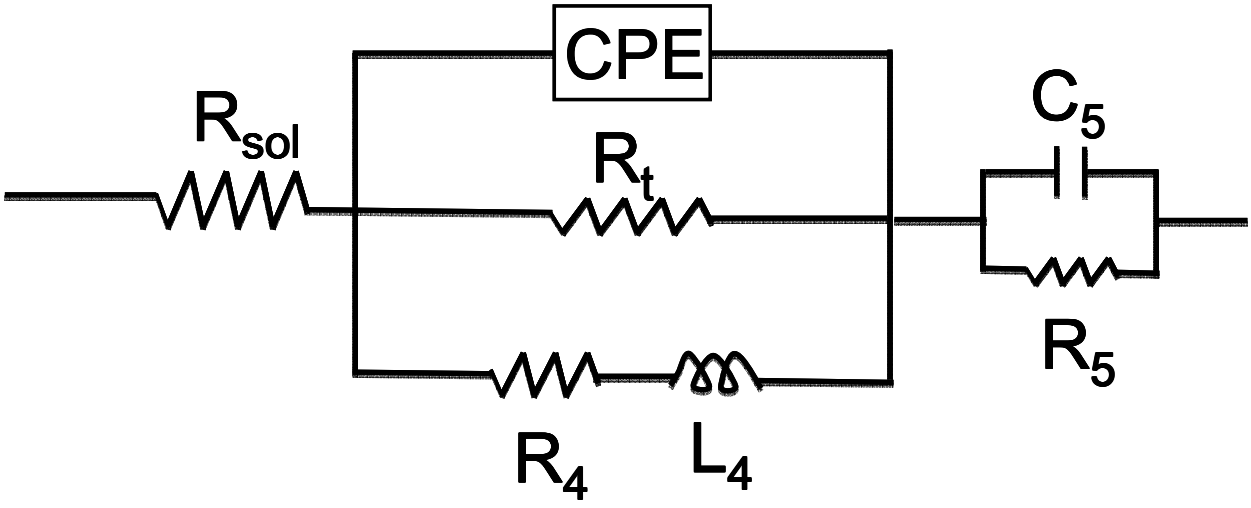

Fig. 5b

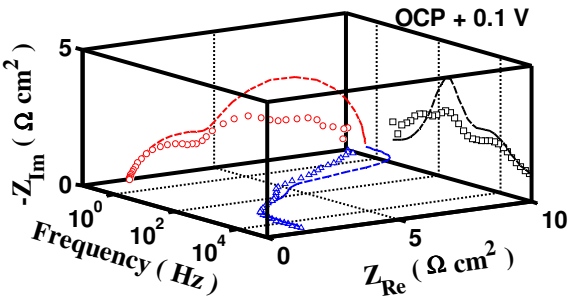

Fig. 6(a)

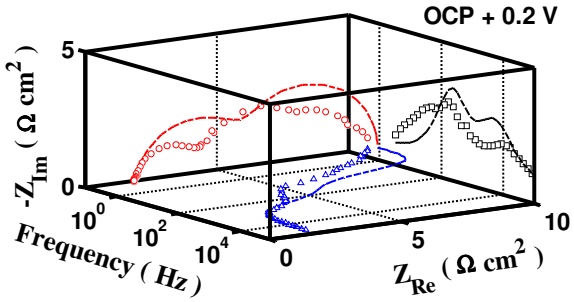

Fig. 6(b)

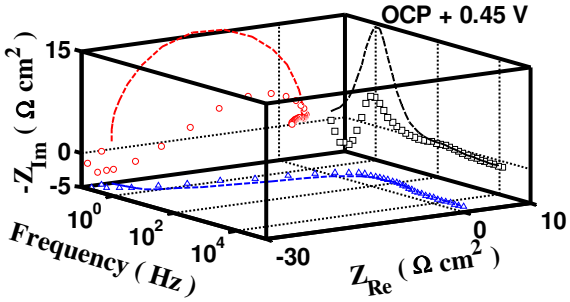

Fig. 6(c)

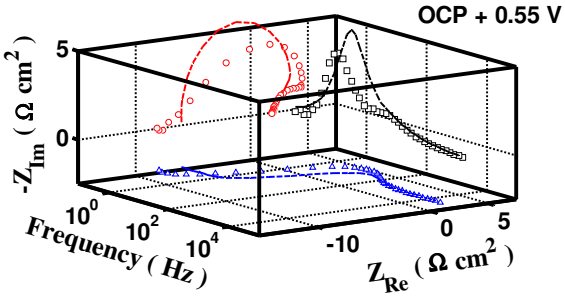

Fig. 6(d)

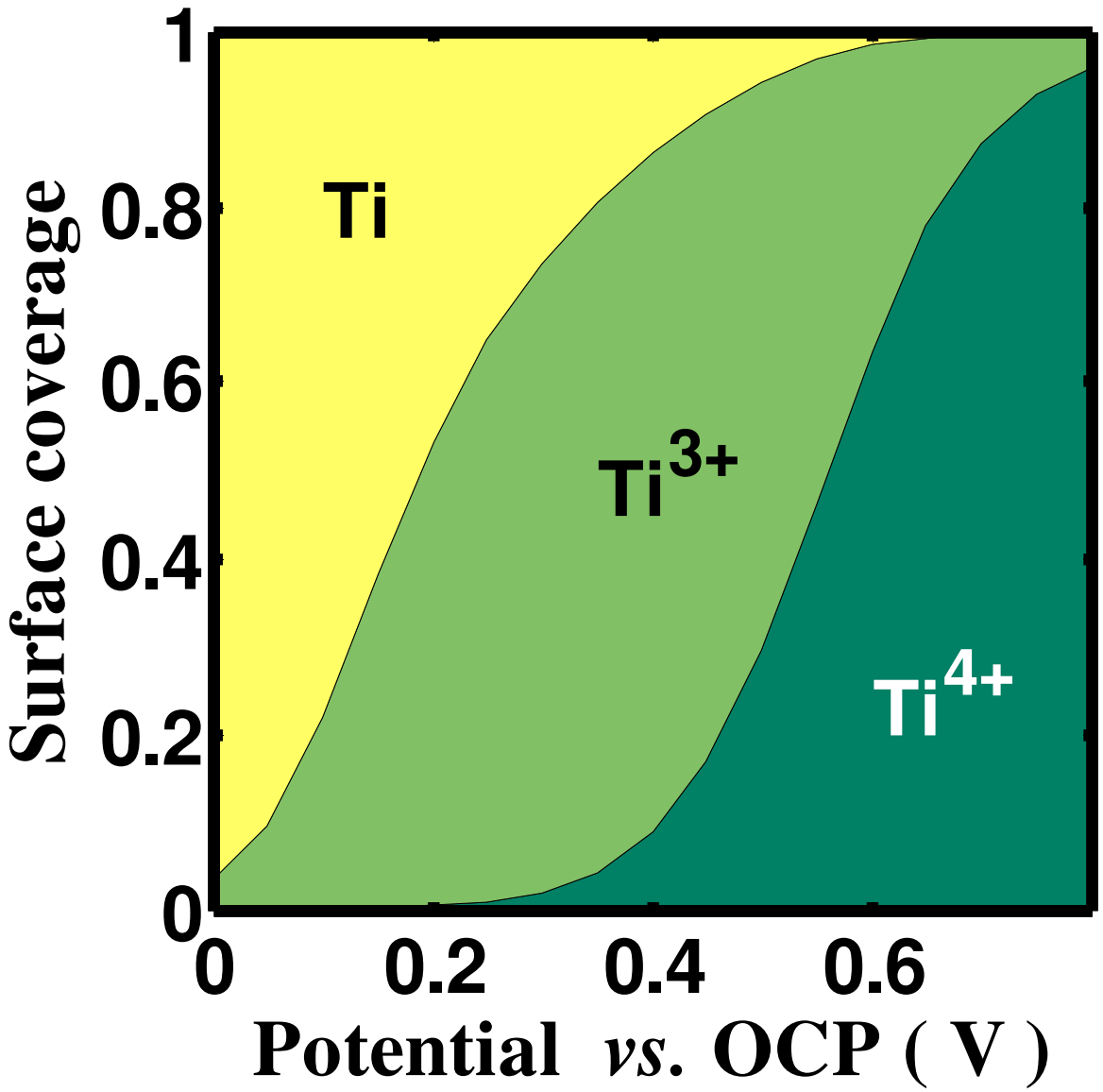
Surface coverage
1
0.8
0.6
0.4
0.2
0
Ti
Ti3+
Ti4+
0
0.2
0.4
0.6
Potential vs. OCP (V)

Fig. 7

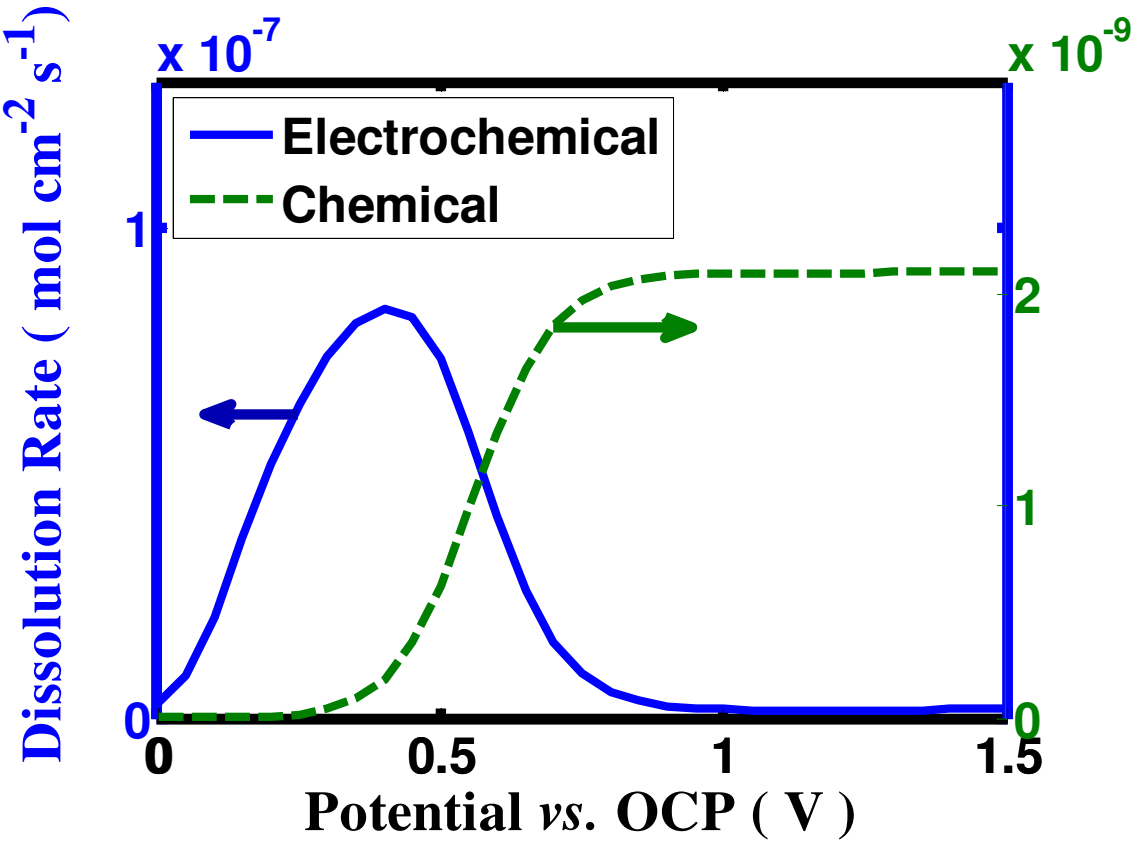
x 10^-7
x 10^-9
Electrochemical
Chemical
Dissolution Rate (mol cm^-2 s^-1)
Potential vs. OCP (V)
0
0.5
1
1.5
0
1
0
1
2

Fig. 8